Available online at www.sciencedirect.com
SCIENCE DIRECT®
Journal of Sound and Vibration 275 (2004) 1113–1126
JOURNAL OF SOUND AND VIBRATION
www.elsevier.com/locate/jsvi

Letter to the Editor

An assessment of modal property effectiveness in detecting bolted joint degradation: theory and experiment

M.D. Todd[a,*], J.M. Nichols[b], C.J. Nichols[c], L.N. Virgin[c]

[a] *Structural Engineering Department, University of California at San Diego, La Jolla, CA 92093-0085, USA*
[b] *U.S. Naval Research Laboratory, Code 5673, Washington, DC 20375, USA*
[c] *Department of Mechanical Engineering and Materials Science, Duke University, Durham, NC 27708, USA*

Received 24 January 2003; accepted 22 October 2003

1. Introduction

The capability to assess the functionality of a given structure or sub-system is tremendously important to the civilian and military communities. Economic pressures, enhanced performance requirements, liability issues, and other factors force structural owners to consider strategies for reducing operational costs, including maintenance. Historically, such strategies have relied upon human inspection or rigid maintenance schedules with little regard to more automated methodologies. With the rapid advances in sensor technology, structural materials, and data processing and management, structural owners have increasingly embraced research and development in advancing the field. A good example of the evolving approaches taken by structural owners is the United States Navy, which has begun to transition the maintenance of all of its civil, marine, and aerospace structures towards a condition basis. This means that maintenance and structural assessment will be done as necessary, not at a fixed schedule. Such a paradigm shift, especially when coupled with reduced man-power initiatives, requires the development of advanced, automated methods for assessing the health of the structure.

Several approaches have been developed over the last several decades within the traditional non-destructive evaluation (NDE) field, such as radiography, thermography, and ultrasonic inspection; an overview of such techniques may be found in Ref. [1]. Researchers have also turned to the vibration domain, where some characteristic "features" from the structure's vibration response are analyzed for indications of damage or degradation. In the vibration domain, the majority of the literature has considered features derived from a modal analysis of the structure, e.g., resonant frequency shifts, mode shape shifts, modal damping changes, flexibility, etc. The literature expanse in this area is too vast to cite here, even representatively. A relatively recent

*Corresponding author. Tel.: +1-858-5345951; fax: +1-858-5346373.
E-mail address: mdt@uscd.edu (M.D. Todd).

0022-460X/$ - see front matter © 2003 Elsevier Ltd. All rights reserved.
doi:10.1016/j.jsv.2003.10.037

good summary of various applications of modal-based methods to a wide variety of structural assessment scenarios may be found in Ref. [2].

One structural sub-system studied frequently in the literature is moment-resisting connections, often characterized by threaded fastener assemblies. Threaded fasteners are popular due to advantages such as the ability to develop a clamping force and the ease with which they may be disassembled for maintenance. It has been well documented that such fasteners loosen under shock, vibration, or thermal loading, and a recent comprehensive discussion of these effects is given in Ref. [3]. One recent excellent work presented a combined finite element and experimental study of dynamic shear loading-induced loosening and showed that the minimum load required to initiate loosening is lower than previously reported [4].

Because of the highly localized nature of bolt loosening and failure, most approaches in this field have involved two- and three-dimensional finite element formulations, e.g., Refs. [5–7]. These approaches are well suited to studying the fundamental nature of the problem and guiding the design process. From a vibration domain structural monitoring perspective, the question is whether these loosening effects may be detected indirectly through vibration measurements and modal analysis of the vibration. In this work, an experiment and a corresponding simple model are constructed to explore whether modal analysis (in terms of resonant frequencies and mode shapes) is an appropriate tool for such a problem. A beam is bolted to supports at its edges, but springs encase the bolts such that greater control over the clamping force is retained for study purposes. In other words, the addition of a spring, while not an element normally added to such joints in practice, facilitates much more precise user control over the effective preload that may be placed on the connection. A simple non-linear model is proposed that globally describes the strength of connection of the beam to its base in terms of an elastic boundary condition stiffness. This approach assumes that only loads perpendicular to the axis of the joint are applied (no shearing), and consequently the effects of friction are not included. Overall, the purpose is to provide a very simple model that globally describes the connectivity condition in a generic way in the joint, and it is not the intent to model specific local behaviors within the joint. The overall goal is to assess to first order whether a vibration-based modal analysis may be used to assess joints subject to simple connectivity (clamping force) loss where the connectivity is modelled by a simple non-linear stiffness function.

With this focus in mind, the transition from fully clamped to fully free is implemented at one edge, and a modal analysis is performed at various steps along the way. We show that resonant frequencies and mode shapes are relatively insensitive to clamping force changes over wide ranges with a narrow region of sudden transition where there is greater sensitivity. This lack of "smoothness" in transition suggests that modal properties may not be ideal features to use in bolted joint health monitoring, especially from a prognostic point of view.

2. The model

2.1. Elastic boundary constraints

The overall system to be modelled is a thin aluminum beam. The equation governing free vibrations of an Euler–Bernoulli beam is given by

$$w_{xxxx} + w_{tt} = 0, \tag{1}$$

where $w(x,t)$ is the vertical displacement non-dimensionalized by beam length L, x is the axial position coordinate along the beam non-dimensionalized by beam length L, and t is time non-dimensionalized by $\sqrt{\rho AL^4/EI}$, where ρ is the beam mass per unit volume, A is the cross-sectional area, E is Young's modulus, and I is the area moment of inertia. All properties are assumed uniform along the beam.

For a beam whose ends are fastened by bolts, the exact boundary conditions are very complicated, as evidenced from the details of the finite element studies cited in the first section. The main purpose in developing a model in this work is to capture the most simple relevant behavior describing the loss of clamping force on the beam boundary as the fastener loosens, without regard to the exact mechanism of loosening or localized details of the process evolution. A quasi-linear model utilizing generalized elastic boundary constraints is proposed that captures this behavior and matches well with experimental observations (to be presented later). In contrast to detailed finite element approaches, this approach is computationally inexpensive and provides a convenient "testbed" for assessing whether various features (such as modal properties) are appropriate for clamping force reduction.

Indeed, elastic constraint boundary conditions could be construed as the most general linear boundary condition, as specific familiar boundary conditions such as "clamped" or "free" may be easily derived from limiting cases of these general elastic constraints. Variations on elastic-type formulations have been used in the literature previously for other purposes, e.g., Ref. [8]. Fig. 1 shows the boundary of a beam subject to general linear elastic constraints in shear, denoted by the K_V spring, and in moment, denoted by the rotational K_M spring. A static moment and y-direction force balance acting on the typical edge element shown is [9]

$$\sum F_{y\text{-direction}} = 0 = -V + K_V L w, \quad \sum M_o = 0 = M - K_M w_x - VL\,\mathrm{d}x, \tag{2}$$

where forces in moments in other planes are ignored and the usual linearity assumptions implicit in Euler–Bernoulli theory are maintained for model consistency. As $\mathrm{d}x \to 0$ in the limit, the general boundary conditions for the moment M and shear force V, applicable at the boundaries, are thus

$$M = K_M w_x, \quad V = -K_V L w. \tag{3}$$

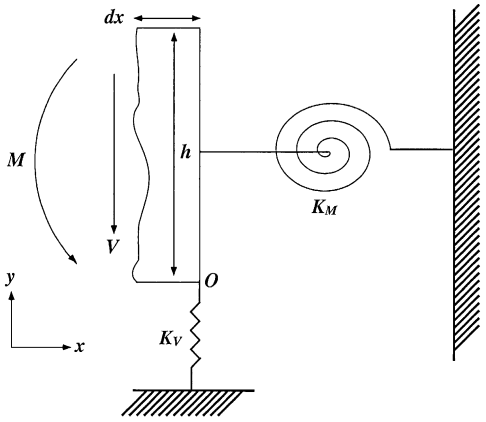

Fig. 1. Elastic edge constraints for an Euler–Bernoulli beam.

For Euler–Bernoulli beams, the internal bending moment and shear force are given by

$$M = -\frac{EI}{L} w_{xx}, \quad V = -\frac{EI}{L^2} w_{xxx}. \tag{4}$$

Equating Eqs. (3) and (4), the elastic boundary constraints may be re-expressed as

$$w_{xx} = -\alpha w_x, \quad w_{xxx} = \beta w, \tag{5}$$

where $\alpha = K_M L/EI$ and $\beta = K_V L^3/EI$. As both K_M and K_V approach zero in the limiting case ($\alpha, \beta \to 0$), the classical free end boundary condition is obtained. As these values approach infinity ($\alpha, \beta \to \infty$), the classical clamped end boundary condition is obtained.

The values of α and β in a purely linear formulation would be constants, as they reflect the stiffness values of the respective springs. Bursi and Jaspart [6], however, showed how the clamping force and clamping moment present in a fastener are strongly non-linear functions of fastener axial strain during transition from the elastic to inelastic regime. The slopes of the force/displacement and moment/rotation curves presented in their work reflect the effective stiffness present, and the dominant characteristic of these curves is that the slope is initially extremely large and goes to zero as the forces and moments saturate during initial plastification. This non-linearity may be readily incorporated into the current model by allowing α and β to be modified by an appropriate function that trends to reflect the elastic-to-plastic transition of a fastener assembly. This function, denoted by K, is proposed to be of the form

$$K(f) = \tanh(\kappa f)\left[p + (1-p)\tanh\left(\kappa \frac{1-f}{f}\right)\right], \tag{6}$$

where κ and p are tuning parameters, and f is a measure of the ratio of the clamping force (or moment) to the maximum clamping force (or moment). A series of these functions for $p = 2$ and various κ is shown in Fig. 2. The p parameter primarily adjusts the magnitude of the stiffness function at $f = 1$, which corresponds to the maximum clamping force or moment possible (both theoretically infinite in the idealized "fully clamped" boundary condition). The κ parameter

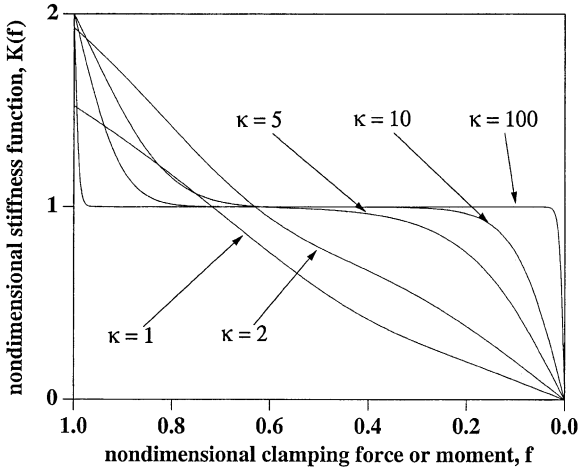

Fig. 2. Proposed non-linear stiffness function $K(f)$ used to describe the clamping force transition.

adjusts the rate at which the stiffness changes, particularly at extremes in clamping force near the minimum ($f = 0$) or the maximum ($f = 1$). It should be noted that the horizontal axis is plotted in reverse, to indicate that normally a fastened joint begins life at maximum clamping force and moment and loses that functionality over time as discussed previously.

It is noted that the stiffness function, particularly at larger κ, is flat for a large spectrum of non-extreme clamping loads. In the experiment to be discussed shortly, springs were used in place of fasteners so that better control of the clamping force was retained. The springs themselves are fairly linear over a wide region of compression, but as the extremes of a fully compressed state or a fully non-compressed state are approached, the springs behave non-linearly with rapid effective stiffness changes over a very short distance. This behavior exactly mimics the function K, particularly for larger κ: the springs behave linearly over a wide region ($K = 1$ in that region) with rapid effective stiffness increases and decreases at full compression and no compression. For perfectly idealized linear springs, K would be unity for all clamping forces or moments. Thus, the expressions for the boundary conditions in Eqs. (5) could be modified to give

$$w_{xx} = -K_\alpha \alpha w_x, \quad w_{xxx} = K_\beta \beta w, \tag{7}$$

where the nominal stiffnesses α and β have been modified by corresponding functions K_α and K_β to reflect the non-linear stiffness effects. In this reformulation, α and β are now interpreted as constants that scale the flat region of K, and all stiffness variation is contained within K. These boundary conditions, with the new non-linear stiffness function, are now not easily satisfied, because the function K varies as w changes during vibration (i.e., the non-linear stiffness function depends on the displacement w itself). However, if the vibrations are assumed small, then no appreciable stiffness change occurs during the vibration except at the very extremes of the spring compression range. Thus, a "quasi-linear" boundary condition exists in the sense that for a given initial, static spring compression, K is assumed constant.

2.2. Solution results

Now that the boundary condition model has been established, the problem may be solved by usual modal expansion methods. In the experiment, the springs were controlled at only the $x = 1$ boundary, the springs at $x = 0$ were left fully compressed such that the idealized clamped boundary condition applies. Assuming that $w(x, t) = \phi(x)e^{ik^2 t}$, Eqs. (1) and (7) are reduced to the eigenvalue problem

$$\phi_{xxxx} = k^4 \phi, \quad \phi(0) = 0, \quad \phi_x(0) = 0, \quad \phi_{xx}(1) = -K_\alpha \alpha \phi_x(1), \quad \phi_{xxx}(1) = K_\beta \beta \phi(1). \tag{8}$$

The solution to this problem is

$$\begin{aligned} \phi(x) &= \sin kx - \sinh kx + C(\cos kx - \cosh kx), \\ C &= \frac{k^3(\cos k + \cosh k) + K_\beta \beta(\sin k - \sinh k)}{k^3(\sin k - \sinh k) + K_\beta \beta(\cosh k - \cos k)}, \end{aligned} \tag{9}$$

where the values of k are taken to be the roots of the characteristic equation

$$\begin{aligned} &K_\alpha \alpha K_\beta \beta + k^4 + k(K_\beta \beta - k^2 K_\alpha \alpha)\cos k \sinh k \\ &\quad + \cosh k((k^4 - K_\alpha \alpha K_\beta \beta)\cos k + k(K_\beta \beta + k^2 K_\alpha \alpha)\sin k) = 0. \end{aligned} \tag{10}$$

It is readily shown that under the idealized limiting cases of fully clamped ($K_\alpha\alpha, K_\beta\beta \to \infty$) and fully free ($K_\alpha\alpha, K_\beta\beta \to 0$) boundary constraints, the characteristic equation reduces to the familiar expressions

$$1 - \cos k \cosh k = 0, \quad 1 + \cos k \cosh k = 0, \tag{11}$$

respectively.

3. Experimental system and procedure

A physical representation of the model is shown in Fig. 3. An aluminum beam measuring 5×10^{-1} m in length, 5×10^{-2} m in width, and 3.175×10^{-3} m in thickness was attached to rigid supports at both ends with a bolt-and-spring assembly as shown. Each spring had a linear spring constant of 64.6 N m^{-1} and relaxed length of 2.0 cm. Four nominally identical spring-and-bolt assemblies were used at each boundary of the beam. On one boundary, all the springs were tightened to a fully compressed condition (nominal spring length of 0.55 cm) such that the

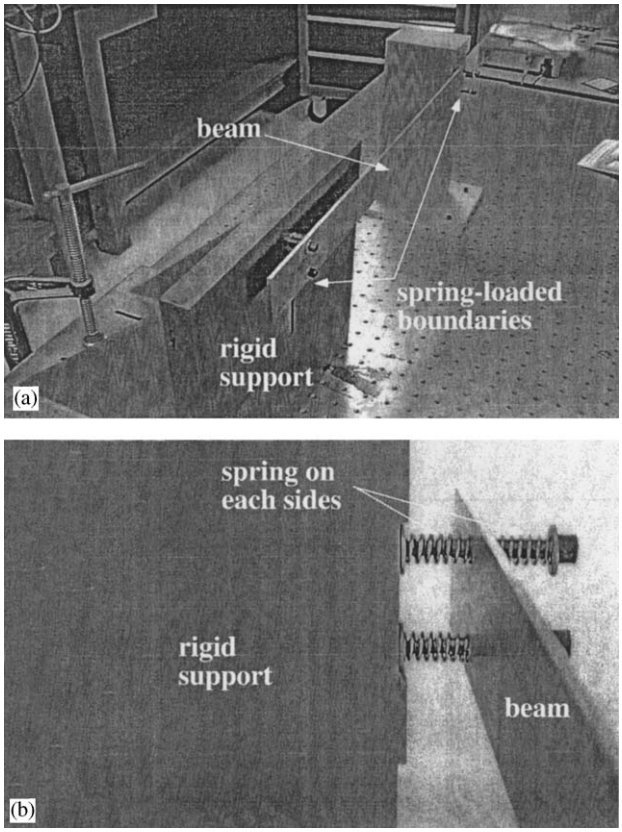

Fig. 3. Photograph of (a) the experimental beam and (b) a close-up photograph of the spring-and-bolt assembly used to control clamping force.

idealized clamped boundary condition was realized. Tightening or loosening the bolts on the other boundary results in compression or elongation of the springs on both sides of the beam and thus serves as a means of controlling the clamping force. Thirteen different compression lengths (clamping force levels) were tested, from the fully compressed state to a final idealized "free" condition, where the springs and bolt were completely removed.

Impact modal testing was performed at each clamping force level, using a multiple-input/single-output (MISO) approach. The beam was divided into equal segments of 5 cm giving a total of 10 points, including the spring-constrained end. The eighth point, located 40 cm from the clamped end, was used to measure the beam's response to impact excitation, while the remaining nine points served as the locations at which the impact was applied. The response location was chosen so as to avoid taking measurements at a node for the first five predicted modes. Excitation was provided by means of an Endevco modal hammer, and response data were acquired using an Ometron VH300+^{TM} single-point Laser Doppler Vibrometer (LDV). Both the excitation and response signals were recorded simultaneously using the PULSE^{TM} Multi-analyzer system from Bruel and Kjaer at a sampling rate of 2048 Hz. The beam was struck ten times at each of the impact locations, and the results were averaged in PULSE to obtain one frequency response function (FRF) using the H_1 estimator for each of the nine excitation/response pairs. As a result of the averaging process, the bandwidth of the sampled data was reduced to 800 Hz. This testing procedure was repeated at each of the clamping force levels for a total of $13 \times 9 = 117$ frequency response measurements. For each FRF, a peak detection algorithm was used to track the first five resonant frequencies. Although frequency information alone could have been extracted with a single-input/single-output (SISO) approach, the current method is required for obtaining mode shape data. Mode shape estimates were obtained by means of an eigensystem realization algorithm [10]. In this procedure, each of the nine FRFs were used to build a state-space model of the dynamics, and the eigenvectors of the state matrix may be scaled to obtain the mode shape estimates. In this work, the mode shapes were scaled such that the maximum nodal excursion was unity.

4. Results and discussion

The first five resonances identified by this experimental procedure, along with the corresponding resonances predicted by the model, are shown in Fig. 4 under decreasing clamping force ρ (non-dimensionalized by EI/L^2). Similarly, the first five mode shapes are shown in Figs. 5–9. For the springs and beam used, $\beta = 1.71 \times 10^1$. Little moment resistance was observed by the bolt-and-spring assembly except near the full compression state, so α was made arbitrarily small (order 10^{-7}); in this way, the moment resistance effects will only be significant near the fully compressed state. For both stiffness functions K_α and K_β, the tuning parameters were chosen to be $p = 2 \times 10^8$ and $\kappa = 25$ to give a large clamping force and moment at the full compression level and considerably rapid transition at the stiffness "boundary layer" extremes (full compression and no compression, or no springs at all).

The experimental and predicted frequency and mode shape data match very well across the full clamping force range. Fig. 4 is plotted with decreasing non-dimensionalized clamping force from left to right, again to imply the normal transition of fastener joints from maximum clamping to

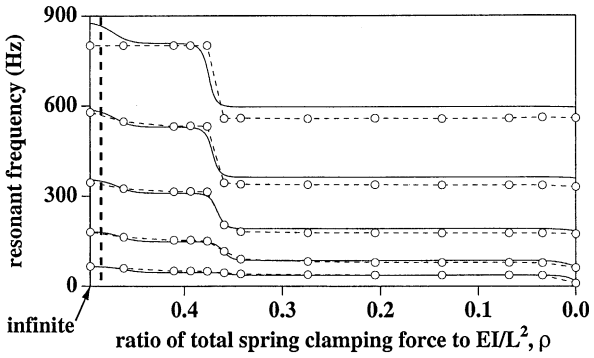

Fig. 4. The trend in the first five identified resonant frequencies as the clamping force is varied. Solid lines indicate theory and dashed lines with unfilled circles indicate experiment.

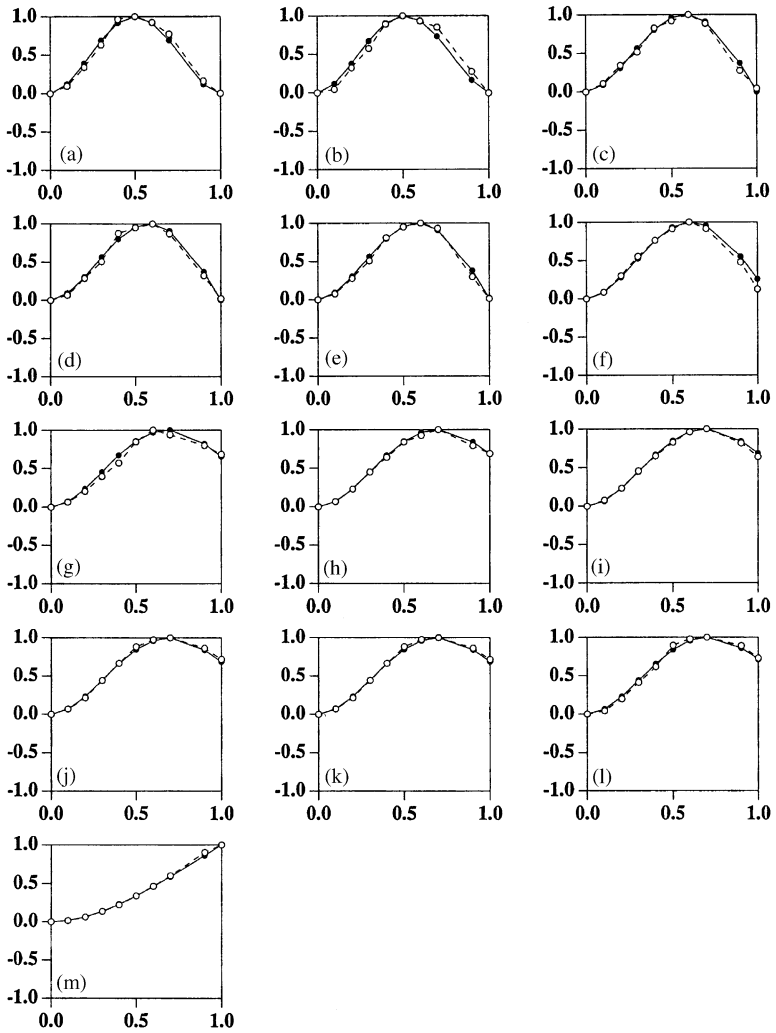

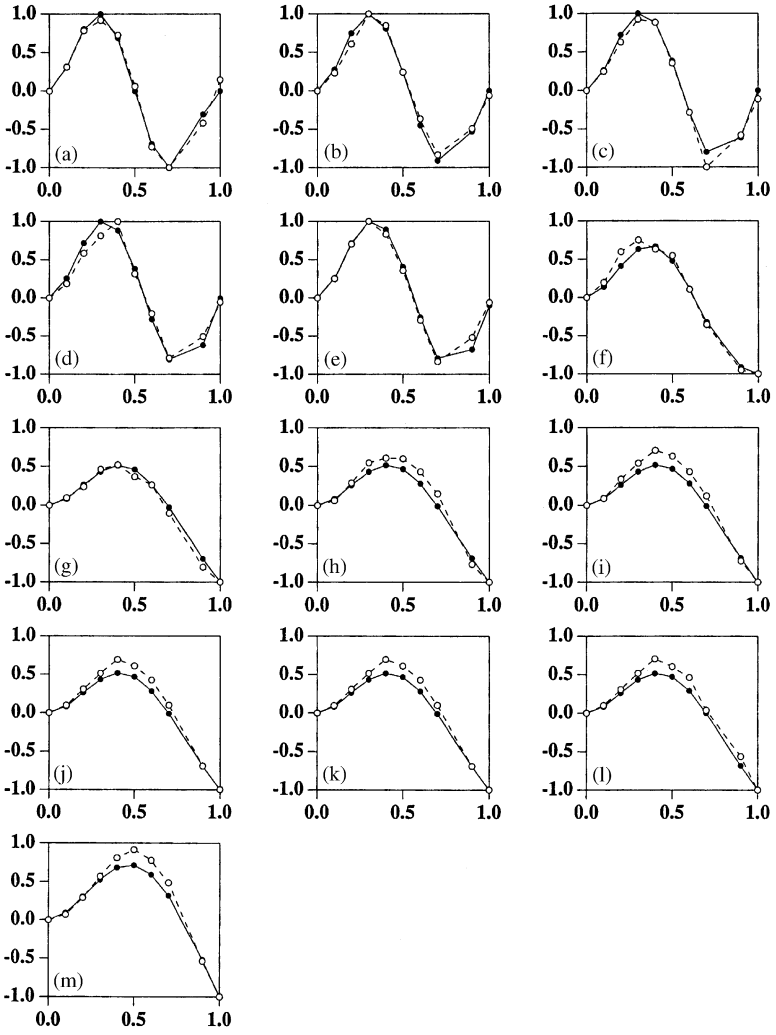

Fig. 6. The trend in the second identified mode shape as the clamping force is varied: (a) $\rho = \infty$; (b) $\rho = 0.46$; (c) $\rho = 0.41$; (d) $\rho = 0.39$; (e) $\rho = 0.37$; (f) $\rho = 0.36$; (g) $\rho = 0.34$; (h) $\rho = 0.27$; (i) $\rho = 0.21$; (j) $\rho = 0.14$; (k) $\rho = 0.07$; (l) $\rho = 0.03$; (m) $\rho = 0$. Solid lines with filled circles indicate theory and dashed lines with unfilled circles indicate experiment.

progressively loosened conditions. The lack of agreement in the fifth resonance at large clamping loads is due to hardware limitations; the 800 Hz Nyquist frequency in the experiment was not sufficient to identify that resonance at the higher clamping levels. As the clamping loads are reduced, the frequencies do not change significantly and then rapidly drop as a critical clamping

Fig. 5. The trend in the first identified mode shape as the clamping force is varied: (a) $\rho = \infty$; (b) $\rho = 0.46$; (c) $\rho = 0.41$; (d) $\rho = 0.39$; (e) $\rho = 0.37$; (f) $\rho = 0.36$; (g) $\rho = 0.34$; (h) $\rho = 0.27$; (i) $\rho = 0.21$; (j) $\rho = 0.14$; (k) $\rho = 0.07$; (l) $\rho = 0.03$; (m) $\rho = 0$. Solid lines with filled circles indicate theory and dashed lines with unfilled circles indicate experiment.

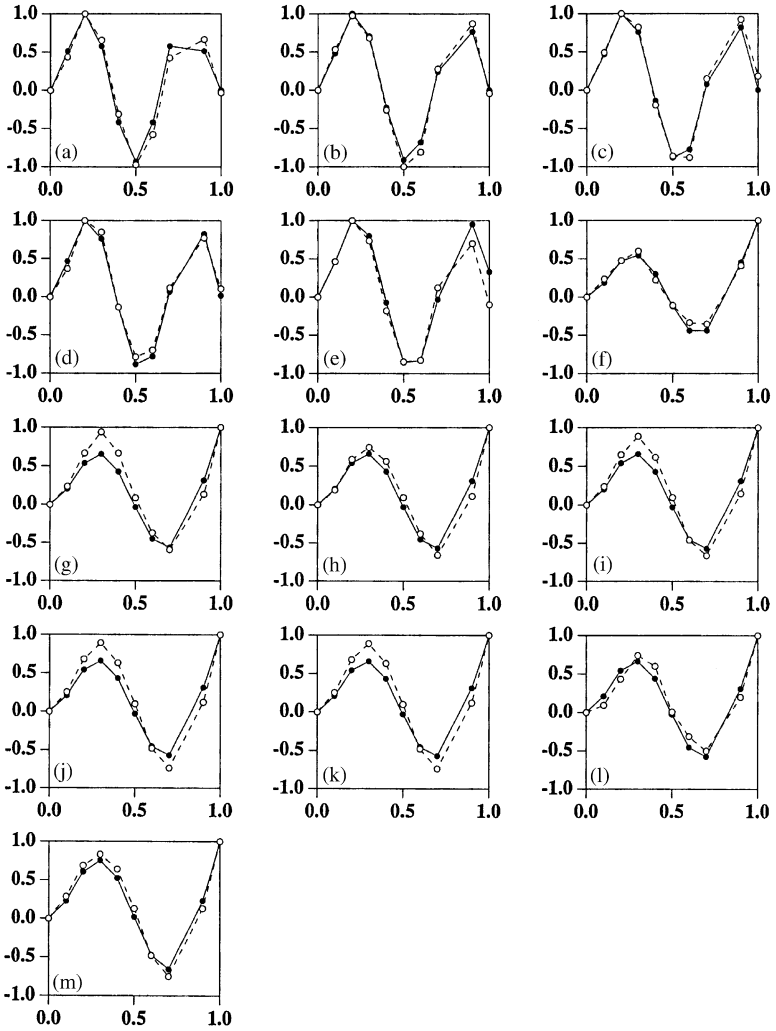

Fig. 7. The trend in the third identified mode shape as the clamping force is varied: (a) $\rho = \infty$; (b) $\rho = 0.46$; (c) $\rho = 0.41$; (d) $\rho = 0.39$; (e) $\rho = 0.37$; (f) $\rho = 0.36$; (g) $\rho = 0.34$; (h) $\rho = 0.27$; (i) $\rho = 0.21$; (j) $\rho = 0.14$; (k) $\rho = 0.07$; (l) $\rho = 0.03$; (m) $\rho = 0$. Solid lines with filled circles indicate theory and dashed lines with unfilled circles indicate experiment.

load is reached. After further load reduction, the frequencies again do not change appreciably, even after the clamping load is completely removed (a free boundary condition). Very similar behavior may be observed in all the identified mode shapes, where again the fifth mode could not be identified at larger clamping forces due to Nyquist limitations. In the mode figures, the clamping force level is indicated by a number in the lower left corner, with "1" meaning fully clamped and "13" meaning fully free.

The sudden transition of the modal parameters at some critical clamping force, with relatively insensitive fluctuation both pre- and post-critical, suggests that resonances and mode shapes may

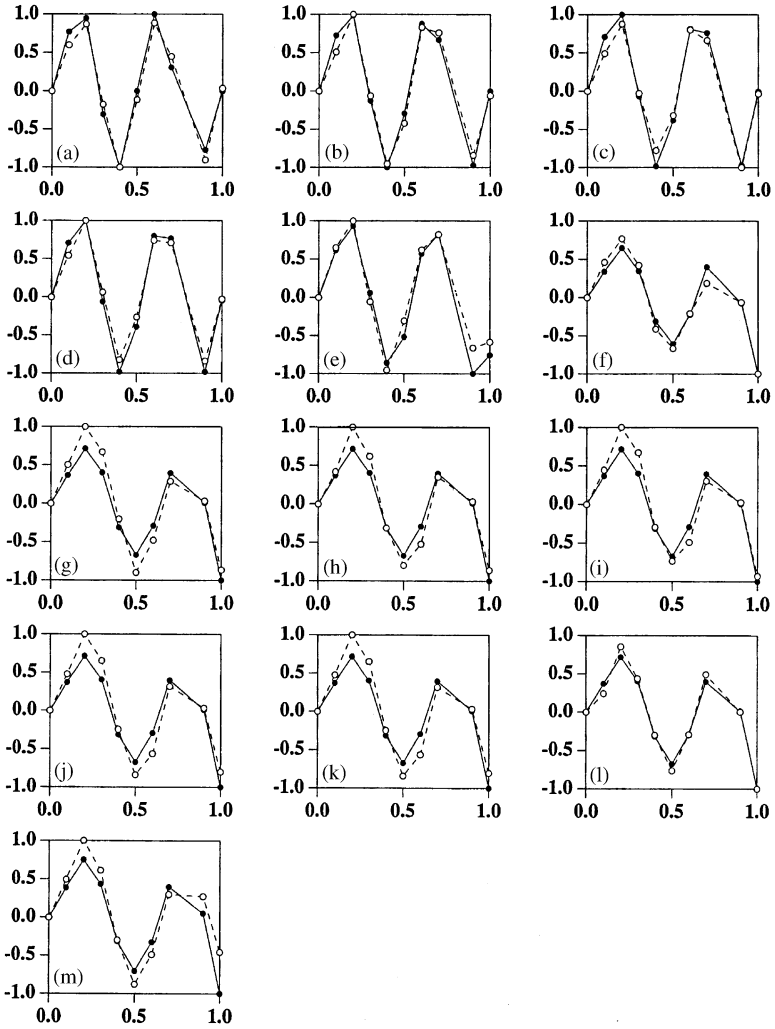

Fig. 8. The trend in the fourth identified mode shape as the clamping force is varied: (a) $\rho = \infty$; (b) $\rho = 0.46$; (c) $\rho = 0.41$; (d) $\rho = 0.39$; (e) $\rho = 0.37$; (f) $\rho = 0.36$; (g) $\rho = 0.34$; (h) $\rho = 0.27$; (i) $\rho = 0.21$; (j) $\rho = 0.14$; (k) $\rho = 0.07$; (l) $\rho = 0.03$; (m) $\rho = 0$. Solid lines with filled circles indicate theory and dashed lines with unfilled circles indicate experiment.

not be ideal candidates for vibration-based structural health monitoring features. Ideal features in this application should typically track linearly or nearly so with the damage scenario (clamping force loss in this study), so that the inverse problem (using the modal properties to classify the joint clamp force) is tractable. The resonant frequencies and mode shapes at the fully clamped condition are sufficiently close to the same properties measured just before the large shift, meaning that there is little ability to classify the data according to clamping force. This would be especially true in a less-controlled environment, where the modal properties may be significantly more "noisy" and less robustly identifiable. In fact, the variability in joint damping with

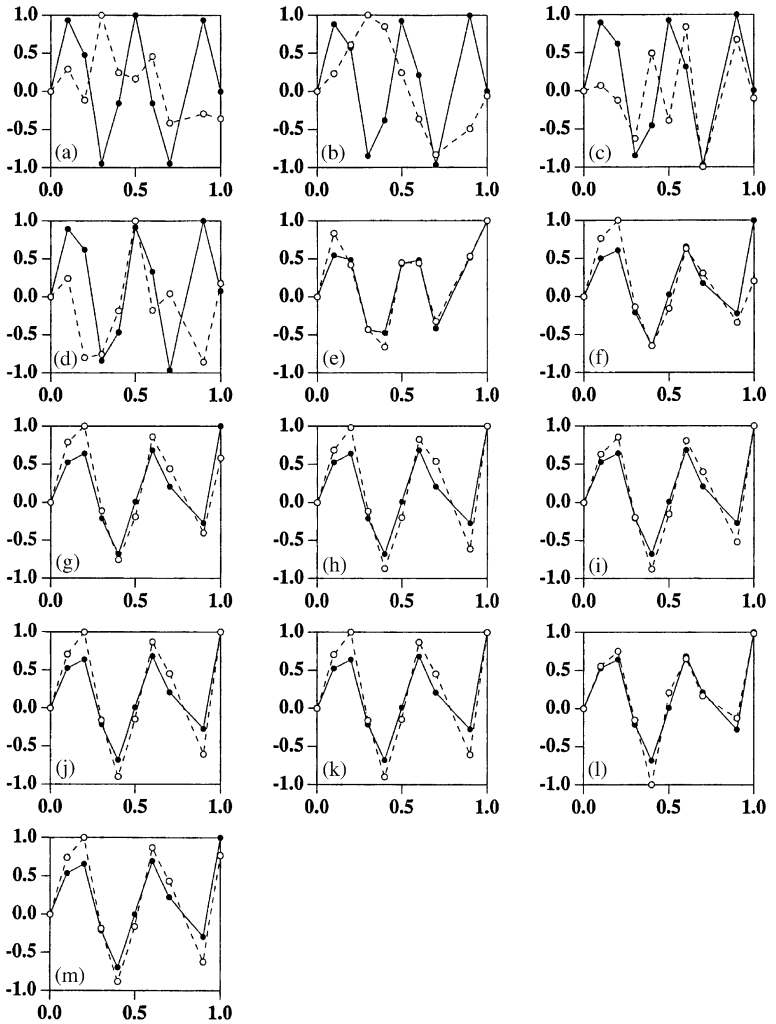

Fig. 9. The trend in the fifth identified mode shape as the clamping force is varied: (a) $\rho = \infty$; (b) $\rho = 0.46$; (c) $\rho = 0.41$; (d) $\rho = 0.39$; (e) $\rho = 0.37$; (f) $\rho = 0.36$; (g) $\rho = 0.34$; (h) $\rho = 0.27$; (i) $\rho = 0.21$; (j) $\rho = 0.14$; (k) $\rho = 0.07$; (l) $\rho = 0.03$; (m) $\rho = 0$. Solid lines with filled circles indicate theory and dashed lines with unfilled circles indicate experiment.

lubrication, environmental condition, and other factors themselves may dominate such that operational variability exceeds changes induced by connectivity loss. Finally, the existence of a sudden shift in the modal properties leaves little recourse for building in safety factors into any prognostic capability which may be developed.

5. Summary

A simple experiment has been conducted on a beam whose boundaries were constrained by fasteners. The fastener joints were modified with springs in such as way as to more precisely

control the clamping force over a wide dynamic range and determine how the beam's global resonances and mode shapes change as the clamping force changes. A simple non-linear model was also developed to describe this behavior, and the model's predictions agreed very well with the experimental observations. The model takes a global joint stiffness approach which seeks only to capture direct clamping force effects and neglects out of plane effects such as friction. Although the model and experiment were conducted under elastic (in a literal sense) loading conditions only, the non-linear stiffness trend matches conditions observed during elastic-to-plastic transition of real bolted assemblies that lead to clamping force degradation. The observed trends in the modal properties suggest that they are relatively insensitive to changes in clamping force, except near a critical clamping force where an abrupt change in the eigenstate occurs. This insensitivity may lead to poor prognostic capability if the modal properties are being used to track joint functionality loss for either maintenance or repair applications.

One possible alternative to modal analysis for detecting joint degradation has been recently discussed in the literature by Nichols et al. [11,12]. This method imparts a chaotic waveform into the structure and builds geometric attractor maps between various sensor pairs. As the joint preload decreases, the subtle relative dynamics induced between the fastened members was detected as an increased error metric describing the ability for one sensor on one side of the joint to predict, or model, a sensor response from the other side. This idea is akin to studying correlation functions, but it is done with state space geometric correlation rather than linear temporal correlation. Results from the cited studies have shown an improvement in minimum load loss detectability over other methods, less energy being input into the structure, and less non-linear progression in the feature with continued degradation.

Acknowledgements

The second author wishes to acknowledge the National Research Council for a post-doctoral fellowship at the U.S. Naval Research Laboratory. The third author wishes to acknowledge the National Science Foundation for a graduate fellowship at Duke University.

References

[1] J.E. Doherty, Nondestructive evaluation, in: A.S. Kobayashi (Ed.), *Handbook on Experimental Mechanics*, Prentice-Hall, Englewood Cliffs, NJ, 1987 (Chapter 12).

[2] S.W. Doebling, C.R. Farrar, M.B. Prime, A summary review of vibration-based identification methods, *Shock and Vibration Digest* 205 (1998) 631–645.

[3] D.P. Hess, Vibration- and shock-induced loosening, in: J.H. Bickford, S. Nasser (Eds.), *Handbook of Bolts and Bolted Joints*, Marcel Dekker, New York, 1998.

[4] N.G. Pai, D.P. Hess, Experimental study of loosening of threaded fasteners due to dynamic shear loads, *Journal of Sound and Vibration* 253 (2002) 585–602.

[5] O.S. Bursi, J.P. Jaspart, Benchmarks for finite element modelling of bolted steel connections, *Journal of Construction Steel Research* 43 (1997) 17–42.

[6] O.S. Bursi, J.P. Jaspart, Basic issues in the finite element simulation of extended end plate connections, *Computers and Structures* 69 (1998) 361–382.

[7] N.G. Pai, D.P. Hess, Three-dimensional finite element analysis of threaded fastener loosening due to dynamic shear load, *Engineering Failure Analysis* 9 (2002) 383–402.
[8] M. Palacz, M. Krawczuk, Vibration parameters for damage detection in structures, *Journal of Sound and Vibration* 249 (2002) 999–1010.
[9] A. Leissa, *Vibration of Plates*, American Institute of Physics, Melville, NY, 1993.
[10] J.-N. Juang, *Applied System Identification*, Prentice-Hall, New York, 1994.
[11] J.M. Nichols, M.D. Todd, M.E. Seaver, L.N. Virgin, Use of chaotic excitation and attractor property analysis in structural health monitoring, *Physical Review E* 67 (2003) 016209.
[12] J.M. Nichols, M.D. Todd, J.R. Wait, Using state space predictive modeling with chaotic interrogation in detecting joint preload loss in a frame structure experiment, *Smart Materials and Structures* 12 (2003) 580–601.